remote sensing

MDPI

Article

Replicability of Digital Terrain Models and Canopy Height Models Derived from Drone Photogrammetry

Jurjen Van der Sluijs [1,*], Robert H. Fraser [2] and Trevor C. Lantz [3]

[1] NWT Centre for Geomatics, Government of Northwest Territories, Yellowknife, NT X1A 2L9, Canada
[2] Canada Centre for Mapping and Earth Observation, Natural Resources Canada, Ottawa, ON K1A 0E4, Canada
[3] School of Environmental Studies, University of Victoria, Victoria, BC V8W 2Y2, Canada
* Correspondence: jurjen_vandersluijs@gov.nt.ca

Highlights

What are the main findings?

- We report the presence of critical dense matching resolution thresholds that affect the replicability of DTM performance in fully vegetated terrain. In our study area, accurate DTMs are most likely when source imagery is acquired with a spatial resolution of $\leq$1.5 cm, side-lap is greater than 80%, and point density is at least 170 m^{-3}.
- Critical dense matching resolution thresholds also exist for CHM metrics, which for Arctic shrublands can be robustly derived across source imagery resolutions <1.5 cm if point clouds are produced at full-scale dense matching, filtered to retrieve the lowest points using simple Triangular Irregular Networks, and have a minimum density of 3219 m^{-3}.

What are the implications of the main findings?

- Hardware and software factors have considerable potential to negatively affect the consistency and replicability of DTM and CHM models in vegetated terrain, challenging the separability of real environmental change from time-series noise.
- Replicability issues have the potential to introduce systematic shifts in estimated properties, influencing conclusions inferred from multi-temporal observations by either overestimating the true changes or making changes undetectable.

Abstract

Replicability of Digital Terrain Models (DTMs) and Canopy Height Models (CHMs) derived from drone photogrammetry is important to understand the extent to which time-series are exposed to methodological noise and conceal real environmental changes. Root mean square error (RMSE) distribution metrics (median/IQR) were used as indicators of replicability across seven drone survey setups, three dense matching scales, and 13 ground point filters in a challenging shrubland environment (total of 273 DTMs and CHMs). We conclude that methodological effects have considerable potential to negatively affect replicability. A power-law relationship between point cloud density and dense matching resolution suggested that important dense matching resolution thresholds exist beyond which replicability degrades considerably. For our Arctic study area, replicability of DTMs (median $\pm$ 0.1 m RMSE Vegetated Vertical Accuracy) and CHMs (within $\pm$0.05 m of true site-level heights) is most likely when source imagery is collected with $\leq$1.5 cm spatial resolution and side-lap of >80%, and if classified point clouds are generated using full-scale dense matching and Triangular Irregular Network filtering. Negative biases for maximum shrub height estimates increased from 4–9% to 14–50% with coarser imagery. We advocate

Check for updates

Academic Editors: Fangning He, Hongzhou Yang, Shengjun Tang, Ding Ma and Ayman F. Habib

Received: 19 December 2025
Revised: 5 February 2026
Accepted: 9 February 2026
Published: 17 February 2026

Copyright: © 2026 by the authors. Licensee MDPI, Basel, Switzerland. This article is an open access article distributed under the terms and conditions of the Creative Commons Attribution (CC BY) license.

for increased attention to drone-derived model replicability to separate real environmental changes from noise during a period of rapid ecological and geomorphic change.

Keywords: point cloud; DTM; CHM; elevation; vegetation; time-series; structure-from-motion

1. Introduction

In the last two decades, aerial drones carrying miniaturized sensors, combined with structure-from-motion (SfM) photogrammetry, have enabled highly detailed three-dimensional environmental reconstructions that extend field-scale observations and fulfill calibration and validation roles for large-area satellite-based mapping [1–4]. Drone systems and sensors have seen rapid uptake due to their flexible deployment and resolution advantages over other sensor technologies. This uptake has transformed the availability of high-resolution Digital Terrain Models (DTMs) and vegetation Canopy Height Models (CHMs), which are fundamental remotely sensed data outputs used in a wide variety of environmental disciplines [5–7]. The use of drones has vastly expanded the range of methods, technologies, and user bases to derive DTMs and CHMs, which were formerly limited to satellite stereo photogrammetry, interferometry, airborne stereo-photogrammetry or LiDAR [8]. More recently, the move from visual line of sight (VLOS) to beyond visual line of sight (BVLOS) drone operations has further expanded methodologies and scales used [9–11].

While the popularity of drone-based surveying has resulted in a growing spatial and temporal footprint of three-dimensional photogrammetric mapping data, these data products have been collected using a wide variety of system setups, flight planning parameters, and post-processing workflows [7,8,12]. This methodological variation is of concern for several environmental monitoring applications as they affect the replicability and generalizability of results [13]. First, the methodological effects are of interest when pursuing local or regional-scale change detection or developing vegetation, biomass, or carbon inventories and monitoring [2,14–18]. Examples of such inventories are local-scale drone plots for observing topographic change due to natural or anthropogenic phenomena and calibrating or validating wall-to-wall subsidence or vegetation estimates derived from satellite data [19]. If the interval between repeated surveys is longer than the operational life of a drone system, they are likely to be conducted using slightly different sensors and/or methods. Replicability between sensors through time is essential for local and regional monitoring [4], as any systematic shifts in estimated properties caused by changing sensors and methods could influence conclusions inferred from multi-temporal observations by either overestimating the true changes or making changes undetectable [20]. For example, shrub height is one of the only physical traits of tundra shrub vegetation that consistently changed in three decades of monitoring [21,22], a change that could be overestimated or obscured if replicability between drone sensors is inadequate. There is thus an urgent need to better understand the replicability of DTMs and CHMs acquired using rapidly evolving drone technology, as drones provide a unique link between field-based research and broad-scale remote sensing studies. This is especially the case in a time when climate change is transforming environments and ecosystems globally [23,24].

Previous studies on drone-derived DTMs and CHMs have focused primarily on achieving maximum accuracy, not data replicability. In response to questions about accuracy, past studies have conducted sensitivity analyses and identified best practices for drone survey design and post-processing to obtain the highest DTM and CHM accuracy possible. For instance, it is generally recommended to use a sufficiently large sensor with a mechanical

shutter, along with a minimum number of ground control points and application-optimized flight altitudes and spatial resolutions [25–27]. Studies have tested the effects of various ground control point configurations on elevation accuracy in bare terrain (Non-vegetated Vertical Accuracy; NVA), yet typically use a single drone and sensor platform at one or a small number of survey altitudes [26,28,29]. Several works have also aimed to identify optimal structure-from-motion (SfM) photogrammetry strategies and ground point filtering methods to improve NVA, with results depending on local vegetation composition and topographic complexity [30–32]. These experimental designs have often been based on testing ground point filtering techniques from a single drone and sensor platform, survey, or GCP setup, raising questions about the generalizability of the findings in other terrain or vegetation settings, or with other hardware configurations. Studies often aim to identify the best combination of platform, sensor, survey parameters, and GCP network to achieve highest model accuracies (in terms of root mean square error; RMSE) for a single monitoring epoch. However, experimental designs are difficult to replicate, and recommendations are sometimes out-of-date as systems and cameras are no longer available or current by the time the research is published.

An emphasis on optimizing accuracies in one location or with one system does not necessarily translate to data replicability or consistent time-series with different systems or survey and post-processing setups in other environmental conditions. This has likely contributed to the range of conclusions regarding which survey altitude or ground point filtering approach to use, illustrating how users may encounter reduced DTM and CHM performance if they operate with other drones or in areas or conditions to which those works were not exposed. To maintain predictive precision across geographic areas, studies typically deploy Airborne Laser Scanning-based DTMs, or GNSS measurements at the base of shrubs, to determine ground elevations needed to retrieve accurate canopy heights [1,33,34]. This is especially necessary in areas characterized by a lack of bare ground patches, and where terrain elevations follow dense ground-covering mats of short dwarf shrubs and moss, i.e., where DTM RMSE reflects Vegetated Vertical Accuracy (VVA). The precision of a methodological approach, expressed as the variability in RMSE (i.e., interquartile range; IQR) of a given method across slightly differing scenarios is therefore just as important to decide on a suitable survey setup and post-processing workflow. It is pertinent to better understand the VVA consistency and replicability of drone-based DTM and CHM models to separate real environmental change from time-series noise introduced via methodological effects.

Novel contributions to the existing literature are needed that address data replicability over multiple epochs rather than simply achieving maximum accuracy at a singular epoch. It is challenging to simultaneously test a variety of drone systems, acquisition parameters, dense matching resolutions, and bare ground classification approaches to better understand the replicability of DTMs and CHMs due to rapidly evolving drone hardware and software. The goal of this work was to test the replicability of DTMs and CHMs across different drone systems, sensors, dense matching resolutions, and bare ground classifiers using a unique dataset serendipitously collected at a shrubland with a complex canopy structure in the Northwest Territories, Canada. Detailed elevation data remains sparse in the circumpolar north due to the high costs of sensor mobilization and challenging logistics and weather across remote environments, yet this information is critical for environmental and infrastructure monitoring or mapping the impacts of climate change. This ongoing need has motivated several field studies to pursue various drone-based applications, such as vegetation, snow, and permafrost degradation [4,9,35], which have also enabled a rare compilation of drone datasets to answer the following three research questions that are relevant across ecological contexts (grasslands, arid shrublands, steppe, forests):

1. How stable are DTMs (as measured by VVA) produced with varying systems, sensors, point cloud densities and bare ground classifiers in vegetated terrain?
2. What is the effect of point cloud density on DTM VVA, and is there an important dense matching scale threshold for shrublands beyond which DTM generation degrades considerably?
3. What is the replicability of shrubland CHMs if DTM stability and other survey parameters are not accounted for?

2. Materials and Methods

2.1. Study Area

This study was conducted at a site 10 km south of Tuktoyaktuk, Northwest Territories, Canada (Figure 1), along the Inuvik–Tuktoyaktuk Highway and within the Tuktoyaktuk Coastal Plain Ecoregion. This ecoregion is a low-relief till plain covered by small lakes and wetlands and is underlain by continuous permafrost with high ground ice content [36]. The climate of the Tuktoyaktuk Coastal Plain Ecoregion is cold and dry (−10.2 °C, 139 mm; means from 1971 to 2000). Mean annual permafrost (ground) temperatures near the Beaufort Sea coast can be below −6 °C [37].

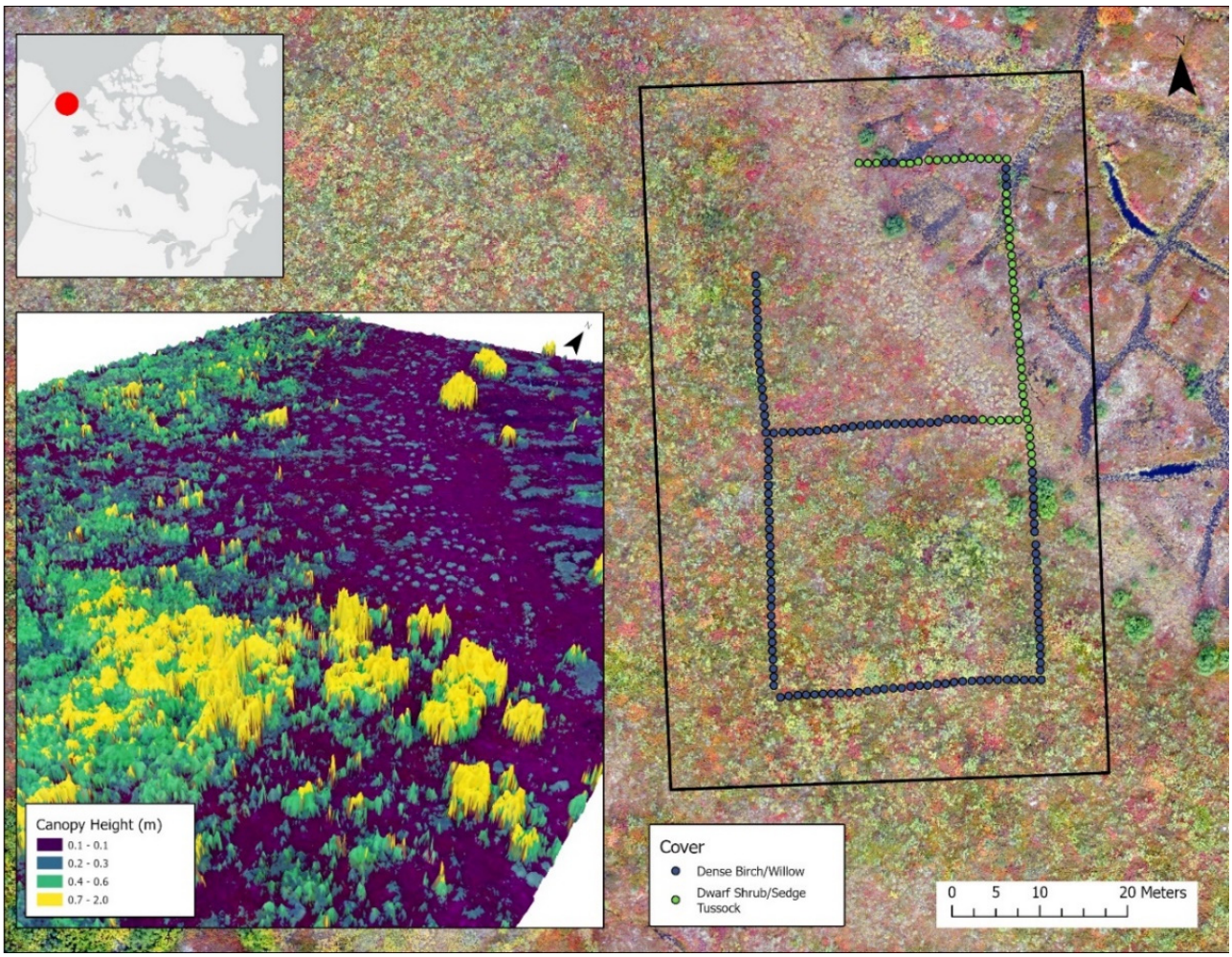

Figure 1. Study location in Northwest Territories, Canada, illustrating site lay-out and ecological conditions with dense birch and willow shrub vegetation as well as high-centered polygonal terrain dominated by dwarf shrubs and sedges. Points show the location of GNSS elevation transects and were clipped to the intersection of all drone surveys. The central and southern East–West transects were used for visual cross-sections of DTMs and DSMs, respectively (Supplementary Materials).

The study site includes two terrain types and vegetation communities: (1) a hummocky upland area of upright dense shrub tundra dominated by birch and willow, and (2) a low-lying area of high-centered polygonal terrain dominated by dwarf shrubs and sedges, where many of the ice wedges have degraded into water-filled troughs (Figure 1). The surveyed area is approximately 2 ha and contains several vegetation types (upright shrub, dwarf shrub, hydrophyllic sedge, and sedge tussock) that are common in the low-Arctic [36]. The largest shrubs are birch (*Betula glandulosa* and *Betula nana*), willow (*Salix* spp.), and alder (*Alnus alnobetula* subsp. *Fruticose* (*Ruprecht*) *Raus*). The dense shrub tundra community is considered mature in the sense that it is near maximum size for the local growing conditions. The shorter statured dwarf shrub community includes bog blueberry (*Vaccinium uliginosum*), lingonberry (*Vaccinium vitis-idaea*), Labrador tea (*Rhododendron subarcticum*), crowberry (*Empetrum nigrum*), and bearberry (*Arctostaphylos rubra*). Common non-shrub vegetation includes cloudberry (*Rubus chamaemorus*), lupin (*Lupinus arcticus*), tussock cottongrass (*Eriophorum vaginatum*), sedges (*Carex* spp.), mosses, and small patches of lichen (*Cladonia* spp. and *Cladina* spp.).

2.2. Data Acquisition

Drone surveys were conducted within a span of 3 years and in the same leaf-on phenological time period, which allowed comparisons across survey setups and datasets with the assumption that the local environment did not change considerably. No signs of disturbance were recorded throughout the period, and annual vegetation growth is typically restricted to 0.5–2 cm/year [22,38,39], or below the expected signal-to-noise of the resultant elevation data. Two quadcopters (Spyder PX8 by XPedition Robotics, Ottawa, ON, Canada, and a Phantom 4 Pro Advanced by SZ DJI Technology Co., Ltd., Shenzen, China) and a fixed-wing system (eBee Plus RTK, senseFly, Lausanne, Switzerland) were flown at various altitudes and overlap settings to capture photogrammetric data from 0.5 cm to 12.5 cm spatial resolution (Table 1; Figure S1). Payloads included an APS-C type mirrorless camera (24 megapixel Sony a6000 with Sony f/2.8 20 mm pancake lens, Sony Group Co., Tokyo, Japan), an integrated 1-inch sensor (20 megapixel DJI FC6310, SZ DJI Technology Co., Ltd., Shenzen, China), and hot-swappable visual (20 megapixel 1-inch) and multispectral (1.2 megapixel) cameras. These payloads were operated under various illumination conditions and solar zenith angles reflecting real-world survey conditions. Photos in JPEG format (for visual RGB data) were captured in shutter priority mode at a 1/1000 s interval, 200–400 ISO, and with focus fixed at infinity. The eBee fixed-wing system was flown in stand-alone mode that prevented the collection of RTK-grade geotag corrections, ensuring equivalence to the quadcopter systems that did not have this capability.

Ground control points were acquired using either a Trimble or Leica dual-frequency GNSS unit (manufacturer-rated precision of 5 mm + 0.5 ppm baseline length) in reference to a locally deployed GNSS base station at an unmarked location. The base locations and ground control points were post-processed to orthometric elevations in NAD83 CSRS UTM zone 8N projection (CGVD13 geoid) using Natural Resources Canada's Precise Point Positioning service (height 95% sigma $\leq$ 2 cm). Reference ground elevations were recorded with GNSS every meter along seven 30 m transects in 2017 to characterize microtopography and to provide independent validation (n = 185). Approximately 40% of the ground measurement points covered areas with dwarf shrub and sedge tussock vegetation, and 60% of the points covered areas containing denser birch and willow shrubs that extended to nearly 2 m in height (Figure 1).

Table 1. Overview of drone surveys. Solar elevations (El), above-ground level altitudes (AGL), and acquisition parameters such as spatial resolution (Res) and the number of ground control points (GCPs) varied through time. Visual examples are shown in Figure S1.

ID [1]	Date (Time) [2]	Conditions	El (°)	AGL (m)	Res [3] (cm)	Photos (no.)	Overlap (For/Side)	System/Sensor	GCP	RMS [4] (m)	Pixel Error [4]
1	31 July 2015 (16:43–16:53)	Mostly cloudy	24	45	0.92	599	90/83	Spyder PX8 Plus 1000, Sony a6000 (RGB)	3	0.001	0.095
2	31 July 2015 (10:06–10:17)	Mostly cloudy	36	90	1.72	531	85/83	Spyder PX8 Plus 1000, Sony a6000 (RGB)	3	0.002	0.137
3	29 July 2017 (17:29–17:39)	Sunny	34	18	0.54	267	80/86	DJI Phantom 4 Advanced (RGB), FC3610	6	0.002	0.122
4	29 July 2017 (15:15–15:54)	Sunny	39	40	1.13	530	80/80	DJI Phantom 4 Advanced (RGB), FC3610	11	0.004	0.086
5	29 July 2017 (16:13–16:31)	Sunny	38	80	2.23	349	86/80	DJI Phantom 4 Advanced (RGB), FC3610	13	0.005	0.115
6	27 August 2018 (13:35–13:55)	Overcast	29	120	2.86	245	90/85	Sensefly eBee Plus RTK, S.O.D.A (RGB)	5	0.004	0.169
7	27 August 2018 (13:07–13:30)	Overcast	28	117	12.47	764	80/80	Sensefly eBee Plus RTK, Sequoia (multispectral)	5	0.01	0.196

[1] Survey IDs 1 and 2 correspond to previously published surveys of Fraser et al., (2016) [35]. [2] Local solar noon at 29 July/31 July and 27 August is 14:58 and 14:53, respectively. [3] Pix4D source resolution may deviate slightly from the spatial resolution setting used for flight planning. [4] Root mean square error measured against GCPs and mean reprojection error (in pixels) after Bundle Block Adjustment (Pix4D Step 1 Quality Report).

2.3. Data Processing

2.3.1. Photogrammetry

The sets of overlapping photos captured during each drone survey were processed using Pix4Dmapper version 4.5.6 software (Pix4D S.A., Lausanne, Switzerland) following a standard SfM workflow [4,35]. For all surveys the same initial processing parameters were used as a data quality control measure to ensure configurations were controlled across experiments (Section 2.4) and that the consistency and independence of model realizations allowed for differences among the factors of interest to be identified (namely hardware differences, dense matching resolutions, ground filter approaches). The standardized parameter configuration calibrated the cameras and completed the bundle block adjustments with assistance of the ground control points (0.5 keypoint image scale, geometrically verified matching, standard calibration, with rematching enabled). Consistent bundle block adjustment results were achieved in terms of georeferencing of RGB surveys based on GCP root mean square error (mean: 0.003 m, st.dev: 0.0014 m) and mean pixel reprojection error (mean: 0.121 pixels, st.dev: 0.027 pixels; Table 1). The consistency of bundle block adjustments meant that subsequent derivatives (i.e., point clouds, DTMs, CHMs) were not sensitive to initial algorithm parameter settings and that the replicability analysis was not biased.

The generation of a wide range of point cloud densities was required to test the effect of point cloud density on model accuracy and to determine whether there is an important dense matching resolution threshold for shrublands beyond which DTM and CHM accuracy degrades considerably. After initial processing using the same bundle block adjustments, each survey dataset was then processed using full-scale, half-scale, and quarter-scale densification image scales (Table 2), with each 3D point requiring a minimum of three correct photo reprojections. The densification image scale defines the scale of the images at which additional three-dimensional points are computed, which together with the point density setting (optimal, high, low) controls the number of points in the final point cloud. To reduce the number of DTM permutations under evaluation, only the default "optimal" point density setting was used, resulting in a computed three-dimensional point for an area constituting the source pixel resolution multiplied by (4/densification image scale) (Pix4D, 2023). The dense matching resolution (D) (Table 2) was then calculated as a multiplication of image source resolution (I), densification image scale (S), and the point density setting, using Equation (1).

$$D = I \times S \times \text{point density setting} \quad (1)$$

Table 2. Overview of dense matching resolutions (D) obtained for each drone survey based on image source resolution (I) and densification image scale (S).

ID [1]	I (m)	S [2]	Point Density Setting	D (m)	Observed Point Density (ρ; m^{-3})
1	0.0092	1	4/(1)	0.0368	15,075
1	0.0092	0.5	4/(0.5)	0.0736	5961
1	0.0092	0.25	4/(0.25)	0.1472	1787
2	0.0172	1	4/(1)	0.0688	2816
2	0.0172	0.5	4/(0.5)	0.1376	838
2	0.0172	0.25	4/(0.25)	0.2752	267
3	0.0054	1	4/(1)	0.0216	76,469
3	0.0054	0.5	4/(0.5)	0.0432	22,312
3	0.0054	0.25	4/(0.25)	0.0864	6668
4	0.0113	1	4/(1)	0.0452	9311
4	0.0113	0.5	4/(0.5)	0.0904	2701
4	0.0113	0.25	4/(0.25)	0.1808	736

Table 2. *Cont.*

ID [1]	*I* (m)	*S* [2]	Point Density Setting	*D* (m)	Observed Point Density (ρ; m^{-3})
5	0.0223	1	4/(1)	0.0892	1222
5	0.0223	0.5	4/(0.5)	0.1784	353
5	0.0223	0.25	4/(0.25)	0.3568	98
6	0.0286	1	4/(1)	0.1144	569
6	0.0286	0.5	4/(0.5)	0.2288	188
6	0.0286	0.25	4/(0.25)	0.4576	49
7	0.1247	1	4/(1)	0.4988	33
7	0.1247	0.5	4/(0.5)	0.9976	8
7	0.1247	0.25	4/(0.25)	1.9952	2

[1] Drone survey IDs in reference to Table 1. [2] Densification image scale set in Pix4D software as either full-scale (1), half-scale (0.5), or quarter-scale (0.25).

2.3.2. Ground Filtering

The seven different drone survey setups and three dense matching scales produced a total of 21 point clouds in LAS format, requiring ground filtering to produce DTMs representing elevations of dense ground-covering mats of shorter dwarf shrubs and moss. Point clouds were imported into a variety of commercial and open-source software programs to gain a better understanding of the variability of DTM outputs as a function of ground filtering or classification technique. A total of 13 approaches were tested, differing between highly automated and custom workflows, various parameterization complexities, and single- or multi-step iterations. Thus, a total of 273 DTMs were generated in this study.

The tested approaches included the selection of the minimum or lowest point (LP) elevation with a 1 m or 2 m window size using ESRI (Redlands, CA, USA) ArcGIS Pro version 3.1 "LAS Dataset to Raster" and linearly triangulating a surface using these points before resampling the TIN to a 1 cm DTM raster output (LP1, LP2). As mentioned by [35], the LP1 and LP2 modeling approach is similar to that of [40] developed for airborne LiDAR analysis and implemented in MicroStation TerraScan (Terrasolid Ltd., Helsinki, Finland). One key difference is that only a single iteration of ground point selection was performed instead of Terrascan's iterative densification of the TIN that adds ground points meeting certain threshold parameters. Pointclouds were also classified in TerraScan using the standard/default settings for photogrammetry (MTSO), as well as LAStool's (rapidlasso GmbH, Gilching, Germany) "Lasground new" with wilderness setting (5 m window size; LGN), to test the difference between single- and multi-iteration selection of ground points.

Three ground point filters available in the open-source Point Data Abstraction Library (PDAL) were also tested using default parameters, including the progressive morphological filter (PMF), a simple morphological filter (SMRF), and a cloth simulation filter (CSF). These filters are based on geometrical principles and are well described [41–43].

A fifth approach was implemented using the ESRI ArcGIS Pro 3.1 "Classify LAS Ground" tool with recent capabilities specifically designed for photogrammetrically derived point clouds. Several parameterizations of this tool were explored: (1) a one-step approach based on a standard/default, conservative, and aggressive setting (PS, PC, PA), or (2) a two-step approach whereby the point cloud was classified using a second iteration with the aggressive setting and re-using the ground-classified points of the one-step approach (PSA, PCA, PAA). For this tool, the conservative setting uses a tighter tolerance on maximum local slope than the standard setting, which captures gradual undulations in topography but ignores sharp relief, while the aggressive setting captures ground areas with sharp relief.

The method of DTM generation was kept constant among MTSO, LGN, the PDAL algorithms and the ArcGIS Pro approaches to isolate methodological effects. Each point cloud was binned and linearly interpolated to a 1 cm spatial resolution DTM using the LAS

Dataset to Raster tool in ArcGIS Pro 3.1, assigning the average value of all ground points in the cell (Figure S1).

2.3.3. Canopy Height Models and Shrub Statistics

Canopy Height Models were created by using a raster differencing workflow by subtracting DTMs against Digital Surface Models (DSMs), similar to Refs. [35,44]. To avoid any unaccounted point cloud noise filtering and smoothing, and to ensure that methodological effects among the trials could be isolated, the DSMs produced by Pix4D were not used. Instead, a DSM representing the upper surface formed by the point cloud was generated for each survey by selecting the point with the largest elevation value in each 1 cm cell, and by linearly triangulating over data voids [35]. After subtracting the DTM from the DSM, any CHM values < 0 m were set to zero since these represented erroneous height values that affect canopy height statistics (Figure S1). Unlike the common practice for treed CHMs, the CHMs in this work were not further smoothed. This preserved complex branching structure typical of many upright shrubs.

Canopy heights for specific shrubs were calculated via an individual shrub detection (ISD) workflow to better understand how shrub height statistics were affected by the replicability of CHMs in shrub-dominated areas. Shrubs were detected using the best-case scenario of highest data resolution (Table 1; Survey 4) and established CHM procedures with known height uncertainties [35]. The ISD workflow was implemented using the R-package ForestTools, which identifies local maxima in a variable window function, a process that is conceptually similar to individual tree detections in boreal forests [45]. The variable window function is a dynamic circular area-of-interest that is different for every pixel as the window radius is based on the CHM pixel height. A function with a radius equal to the CHM pixel value was chosen to reflect that larger shrubs have larger, more complex crowns compared to small shrubs that would otherwise be merged with larger shrubs nearby. A total of 1199 candidate shrub tops were identified based on a minimum height threshold of 0.5 m. A marker-controlled inverse watershed segmentation was used to identify the crown area and diameter corresponding to the candidate shrub tops. The sample of candidate shrubs was further filtered to remove crown areas along data edges, after which crown areas were simplified using a minimum crown area of 2 m, a simplification tolerance of 0.2 m, and the weighted effective area (Zhou–Jones) simplification algorithm using the Simplify Polygon tool in ArcGIS Pro 3.1. The filtering and simplification steps left 299 shrub samples belonging to the two vegetation communities (mean diameter: 1.29 m, SD: 1.53 m) that were used to compare site-level height metrics across the different ground filter approaches, source resolutions, and dense matching settings.

2.4. Experimental Design and Validation

The differences in survey setup, dense matching scales, and ground point filters supported the study objective to investigate the replicability of DTMs and CHMs produced using rapidly evolving systems and sensors. It also allowed us to evaluate the variety of point cloud densities and bare ground classifiers available to end-users. A total of 273 DTMs were evaluated from seven different drone survey setups, three dense matching scales, and 13 ground point filters.

The accuracy of these DTMs was determined using the seven independent ground elevation transects (Section 2.2), from which the RMSE was calculated to measure how well the drone-derived elevations fit the GNSS transects. Due to infrequent true bare ground patches in the study area [35], reported RMSE refers to the VVA as described in [46]. Throughout this work the emphasis was placed on RMSE distributions (through the median and interquartile range) resulting from a given method across slightly differing

scenarios, rather than the highest accuracy obtained in one unique setup scenario. The former represents a better indicator of precision and replicability, important for generating time-series datasets and for deciding on a suitable survey setup and post-processing workflow. Nevertheless, we also report the highest RMSE accuracy to contextualize the findings and to allow for comparisons with previous works.

Metadata on survey information (Table 1), photogrammetric settings (Table 2), as well as the type of vegetation cover and ground filter approach were analyzed in a multiple linear regression framework to test the strength of explanatory variables of observed RMSE. Non-parametric statistical testing (Kruskal–Wallis one-way ANOVA and Dunn's post hoc tests with Bonferroni adjustment) was implemented to assess differences in RMSE among DTM workflows. The relationship between observed point cloud density and dense matching resolution was assessed (both logarithmically transformed to meet assumptions of normality) to determine the usefulness of dense matching resolution as an a priori estimate of point cloud density as well as model accuracy. The R software package (v. 4.0.2) was used to produce descriptive statistics and regression analyses.

To provide a baseline comparison of DTM performance reported in this study, the GNSS GCPs and transect samples were combined (n = 231) to assess the VVA of two archival Airborne Laser Scanning-derived DTMs acquired by McElhanney Ltd. and on file at the NWT Centre for Geomatics. A 2011 survey (Leica ALS60, 200 kHz pulse repetition, Leica, Wetzlar, Germany) produced a DTM using a point cloud with an average 1.7 points m^{-1} first-return sampling density. A 2021 survey (Optec Galaxy T1000, 1 MHz pulse repetition, Teledyne Optech, Toronto, ON, Canada) produced a DTM using a point cloud with an average 35 points m^{-1} first return. After a vertical datum adjustment to the CGVD13 geoid, the RMSE of the 2011 DTM was 0.15 m (or 0.11 m after an additional local bias correction). The RMSE of the 2021 DTM was 0.19 m (or 0.12 m after local bias correction).

Due to the scarcity of tundra vegetation inventory information, there were no representative ground-truthed vegetation height measurements available to validate the CHMs directly for a large shrub sample. For a sample of n = 31 shrubs in the same study area, [35] obtained a R^2 = 0.96 (SE = 8 cm) and a near 1:1 relationship for maximum height measured in the field using a tape measure using a combination of survey ID 1 (Table 1), full-scale matching, and an LP2 ground filter. Similarly, they estimated the average height from six representative upper branches by the mean plus two standard deviations of the CHM values within shrub crown areas (R^2 = 0.91, SE = 11 cm). The 31 shrubs were not used for validation purposes due to the limited sample size, rather the field-validated drone survey and methodology were considered the benchmark for validation purposes. For the 299 shrubs derived through the ISD workflow, we obtained a site-level median estimate of 0.81 m for the maximum height metric and a median estimate of 0.70 m for the average height metric (representing the average height from six representative upper branches). CHM distributions were compared against the benchmark to determine the degree to which estimates would overlap (i.e., replicability of results) or be biased.

3. Results

3.1. DTM Replicability

The varying platforms, sensors and matching densities used in the experimental design resulted in a wide range of point cloud densities, ranging from 2 to 76,500 points m^{-3}, enabling detailed tests of the effect of these densities on DTM and CHM accuracies across five orders of magnitude. Point cloud density (ρ) followed a negative power-law relationship with dense matching resolution (Equation (2), Figure 2a, R^2 = 0.97, $p < 0.001$). The strength of this relationship indicated that datasets generated from different platforms,

sensors, flight altitudes, and post-processing settings can be compared directly using this indicator of dense matching resolution (D).

$$\mathrm{Log}(\rho) = 0.93 - 2.35(\log(D)) \quad (2)$$

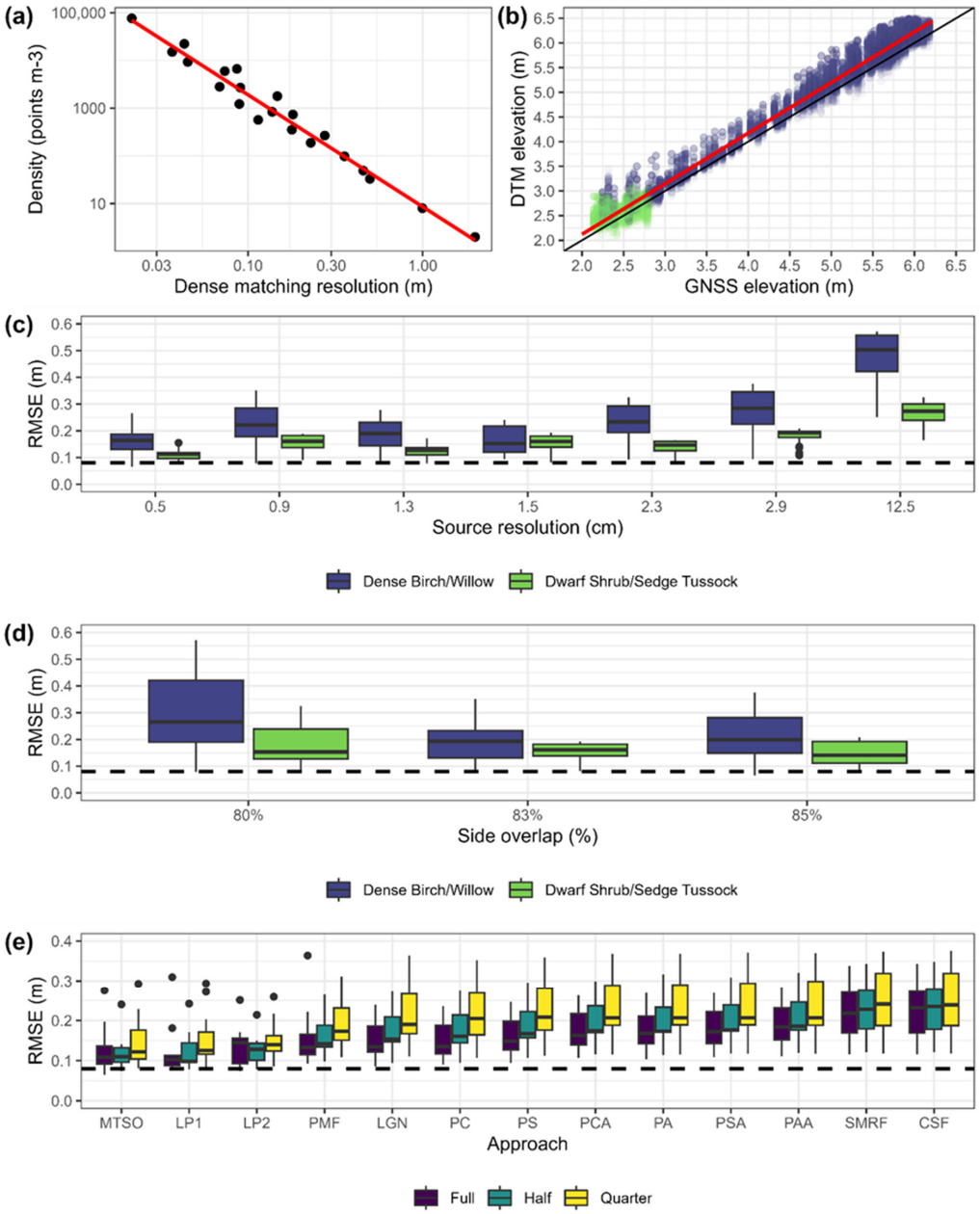

Figure 2. (**a**) Scatterplot of log-normalized dense matching resolution and log-normalized point cloud density; (**b**) scatterplot of GNSS-measured ground elevations against drone-based DTM ground elevations in relation to a 1:1 line, green points show dwarf shrub/sedge patches whereas dense birch/willow patches are indicated with blue points; (**c**) RMSE distributions by resolution of the source imagery and vegetation cover; (**d**) RMSE distributions by side overlap groupings; and (**e**) RMSE distributions for each ground filter approach (x-axis) and densification image scale. Highest DTM accuracy regardless of vegetation cover (0.08 m RMSE, n = 185) represented by dashed line.

Comparisons of all drone-derived DTM elevations against the validation data show a positive bias (+0.18 m, n = 50,505) relative to GNSS transects while following the 1:1 line closely (Figure 2b). More than 83% of the variation in observed RMSEs could be explained by the vegetation cover, source imagery resolution, dense matching scale setting (full,

half, quarter), absolute dense scale resolution, as well as the bare-earth filtering approach ($F(22,523) = 122.2$; $p < 0.001$; Table 3). Vegetation cover was among the strongest explanatory variables of observed DTM RMSE, with higher RMSEs for dense birch and willow patches compared to dwarf shrub/sedges across all source resolution classes. Whereas DTM elevations in dwarf shrub patches were predicted with <0.2 m RMSE no matter the source imagery resolution, elevations near taller dense birch were often modelled with ≥0.2 m RMSE. However, RMSE did not increase with decreasing source resolution from 0.5 cm to 2.3 cm. For example, for dense birch/willow cover no significant differences were observed in RMSE distributions between 0.5 cm and 1.3 cm, 0.5 cm and 1.5 cm, 0.9 cm and 1.3 cm, 0.9 cm and 2.3 cm, as well as between 1.3 cm and 1.5 cm or between 2.3 cm and 2.9 cm (Dunn's $p = 1.0$). Likewise, for dwarf shrub and sedge tussock, no significant differences were observed between 0.5 cm and 1.3 cm, 0.9 cm and 1.5 cm, or between any of 0.9 cm/1.3 cm/1.5 cm against 2.3 cm source imagery (Dunn's $p = 1.0$). At resolutions exceeding 2.3 cm up to 12.5 cm, RMSE was significantly higher than at resolutions <2.3 cm. Variability in DTM RMSE was also higher in drone surveys with 80% side-lap ($n = 3$; Table 1) compared to surveys completed with higher overlap ($n = 4$; Table 1; Figure 2d). Together, these results indicate that source imagery resolution was not the sole driver of model accuracy and highlight that consistent model performance across drone platforms and bare-earth classification approaches can be achieved in this study area if the source imagery has a spatial resolution of <1.5 cm (or <2.3 cm for dwarf shrubs only) and side-laps of >80%.

Table 3. Results of the ANOVA analysis comparing factors influencing RMSE of DTMs.

	Sum of Squares	df	Mean Square	F	*p*
Vegetation cover (*dense birch*, *dwarf shrub*)	0.91774	1	0.91774	501.077	<0.001
Source resolution	2.99819	6	0.49970	272.829	<0.001
Dense matching setting (*Full*, *half*, *quarter*)	0.26350	2	0.13175	71.935	<0.001
Dense scale resolution	0.09865	1	0.09865	53.863	<0.001
Bare-earth approach	0.64591	12	0.05383	29.388	<0.001
Residual	0.95790	523	0.00183		
Total	5.88189	545			

In terms of dense matching settings and ground filters, RMSEs for DTM elevation from full-scale matching results were always lower compared to half-scale and quarter-scale matching (Figure 2e). This clear trend in model accuracy was observed regardless of the bare-earth classification approach, with improvements of up to 5 cm RMSE when dense matching was performed at full scales. Among the ground filter approaches, those based on the lowest point filtering (e.g., MTSO, LP1, LP2) outperformed other filtering techniques. These approaches achieved the highest DTM accuracies at specific survey instances (0.08 m RMSE) as well as the lowest RMSE variability (IQR), indicating these approaches are robust and consistently outperform other methods no matter the source imagery, overlap settings, or dense matching scales (Figure 2e). Improvements were realized for both vegetation cover classes but were especially evident for dense birch and willows (Figure S2). No clear differences in RMSE distributions were observed between dedicated commercially available point cloud software (e.g., MTSO, LGN), general-purpose GIS software (LP1, LP2, ArcGIS Pro options) and open-source software tools. From the open-source PDAL library, the PMF approach consistently achieved better accuracies than the SMRF or CSF approaches, or those available in the ArcGIS Pro suite. Together, the results shown in Figure 2e, Figures S3 and S4 indicate that the variability in DTM accuracy is modulated by

dense matching setting and ground filtering techniques, and that highly consistent results irrespective of survey design can be obtained in this study area with full-scale matching and algorithms focused on TIN-based lowest point filtering.

An evaluation of point cloud densities was required to determine whether there is an important dense matching resolution threshold for shrublands beyond which DTM replicability degrades. DTM RMSE increased considerably beyond a dense matching resolution of 28 cm yet showed only moderate increases for dense matching resolutions up to 28 cm (Figure 3a). Comparison among all ground point filters also showed a noticeable effect of vegetation type (Figure 3a). For the three best-performing ground filters (MTSO, LP1, LP2) there was no effect of dense matching resolution on RMSE up to 28 cm regardless of vegetation type, indicating a robustness of performance regardless of the resolution of the original source imagery (Figure 3b). The absence of a resolution effect indicates that similar accuracies can be expected no matter which of the three ground filters are used for surveys and processing techniques with a maximum dense matching resolution of 28 cm. The lack of vegetation effect also indicated that the three ground filters perform similarly among vegetation types up to this threshold, further increasing generalizability of methods. These results show that there is indeed an important scale threshold beyond which DTM replicability decreases considerably. The 28 cm threshold corresponds to a minimum density of 170 points m^{-3} (Equation (2); Figure 2a).

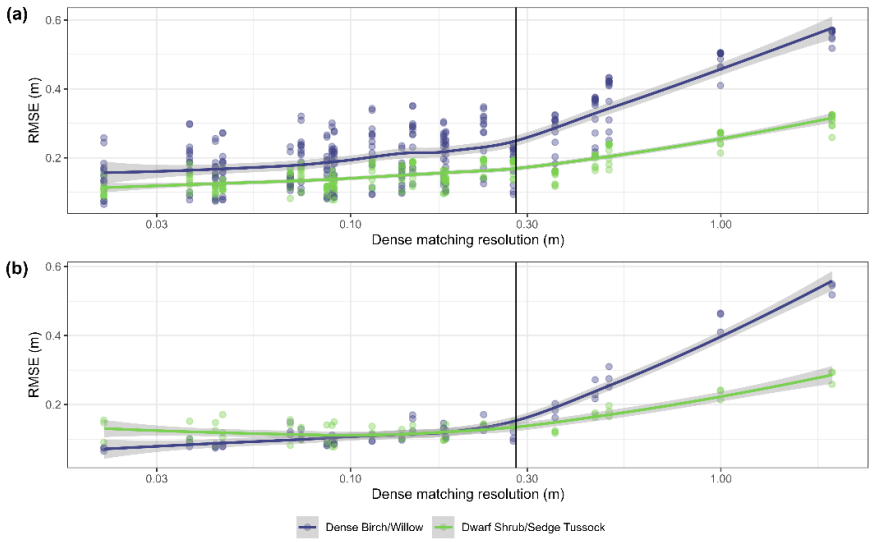

Figure 3. Relationship between dense matching resolution and RMSE by vegetation type. RMSE calculated for unique subsets of ground filtering techniques, dense scales, vegetation cover, sidelap and frontlap: (**a**) all ground filtering techniques, (**b**) three best-performing ground filters (MTSO, LP1, LP2). Locally estimated scatterplot smoothing (LOESS) applied to visualize trends. Gray shading shows the 95% confidence interval of the standard error.

3.2. CHM and Height Metric Replicability

Our results showed considerable methodological effects on CHM-derived height distributions for a large sample of shrubs (n = 299). Maximum height distributions were within ±5 cm of site-level medians using the [35] benchmark for point clouds derived from source imagery spatial resolutions up to 1.5 cm, with full-scale dense matching and LP2 filtering (Figure 4a). Contextualizing this variability to the site-level medians using the field-validated methods from [35] indicated a relative bias of −7% for 0.5 cm imagery, −9% for 1.3 cm imagery, and −4% for 1.5 cm imagery (Figure 4b). Maximum height estimates using either 2.3 cm or 2.9 cm imagery resolution (full scale, LP2) had a bias of −14%, whereas biases of −50% bias were observed for 12.5 cm multispectral imagery (full

scale, LP2). Source imagery resolution therefore plays a considerable role in reproducing site-level vegetation height estimates.

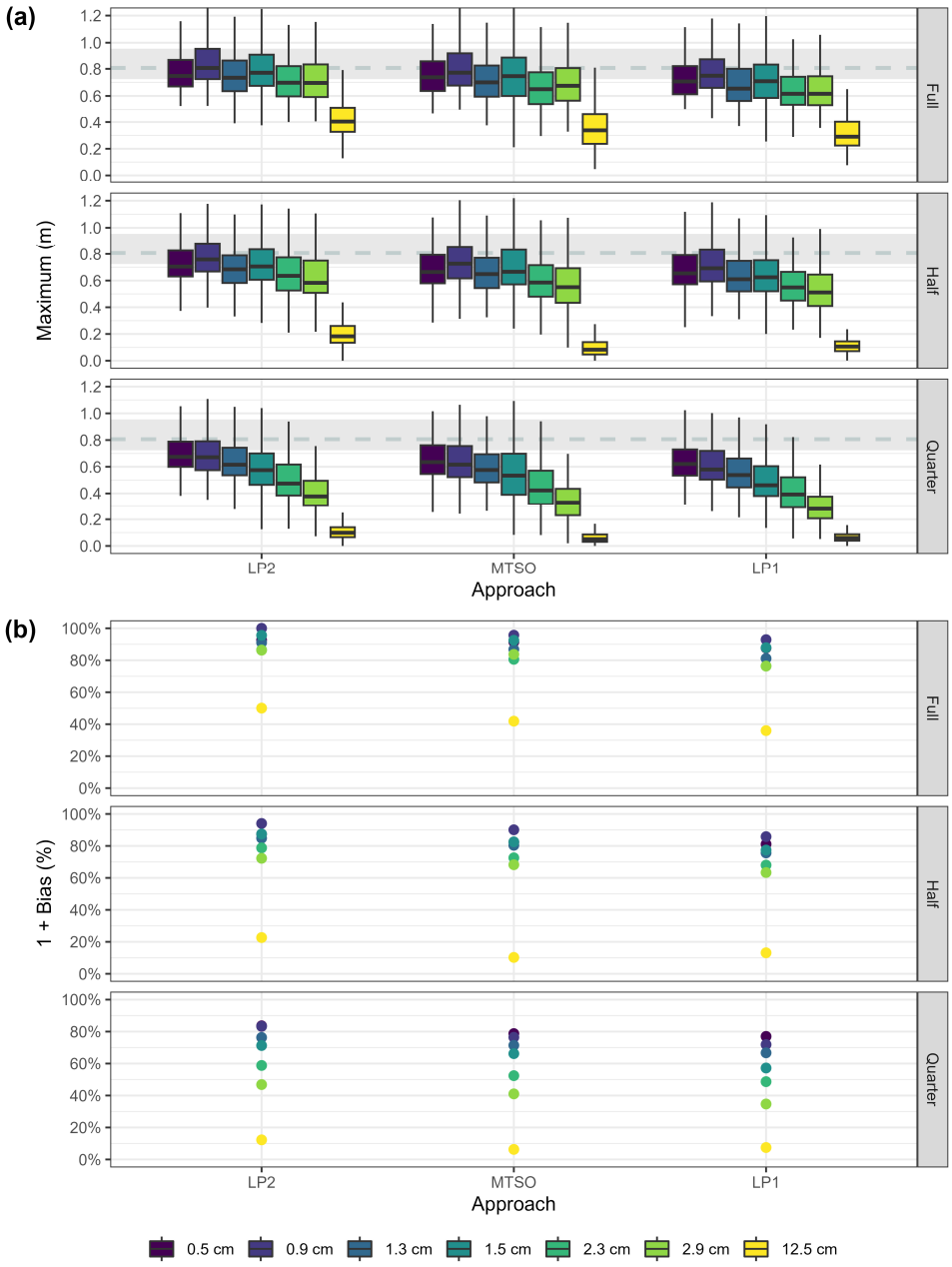

Figure 4. CHM distributions for maximum height of 299 individual shrubs by source imagery resolution, filtering approach and dense matching setting: (**a**) absolute values of the three best filtering approaches, (**b**) values relative to site-level estimates using field-validated methods from [35], expressed as bias. In (**a**) the grey line and grey banner indicate the median and interquartile range of maximum height based on the field-validated methods of [35]. For full figure with other filtering approaches refer to Figure S5.

CHMs produced using the three best-performing ground filters (MTSO, LP1, LP2) had considerably higher site-level maximum canopy heights compared to the other filtering techniques (Figures 4a and S5). This indicates that as DTMs worsened due to suboptimal ground filtering (Section 3.1) so did the CHM accuracy and its derived summary height statistics. Densification image scale also had a pronounced effect on maximum height distributions, as decreases up to 20 cm (−25% bias) and 40 cm (−50% bias) were observed for high-performing ground filters using half and quarter scales (Figures 4a,b and S5).

Results deteriorated further with worsening lower-scale densification filtering results, as biases of −50% to −60% became the norm for half-scale densification and were upwards of −80% for quarter-scale densification (Figures 4a,b and S5). Similar methodological effects were observed in the average height metric (representing the average height from six representative upper branches), but there was a stronger response to worsening ground filtering results or coarsening densification scales (Figure S6). To further illustrate the drivers of shrub height underestimation with coarser imagery, Figures S3, S4, S7 and S8 highlight how positive biases in DTM elevations at the base of shrubs (upwards of 0.5 m at 12.5 cm resolution) propagate into reduced CHM estimates, and that there were only small differences in canopy surface reconstructions (DSM differences ranged between −0.1 m to 0.1 m). These results demonstrate that CHM metrics can be robustly derived across source imagery resolutions <1.5 cm if point clouds are produced at full-scale dense matching and robust ground filtering can be used. If these conditions cannot be met there will be large systematic biases in site-level estimates and issues with temporal consistency of CHM models.

Dense matching resolution was further investigated to better understand if there is an important threshold beyond which CHM metrics degrade considerably. Site-level CHM statistics for maximum height metrics decreased steadily beyond a dense matching resolution of 8 cm, highlighting that there is an important scale threshold beyond which CHM consistency decreases considerably (Figure 5). The 8 cm threshold relates to a minimum density of 3219 points m^{-3} (Equation (2); Figure 2a). For the three best-performing ground filters (MTSO, LP1, LP2), there was little change in observed bias in maximum or average height up to a dense matching resolution of 8 cm (Figure 5). For maximum vegetation height this indicates a degree of robust performance regardless of the resolution of the original source imagery. The absence of an effect shows that vegetation height statistics can be expected to exhibit stable bias no matter which of the three ground filters are used for surveys and processing techniques if the condition of a maximum dense matching resolution of 8 cm is met.

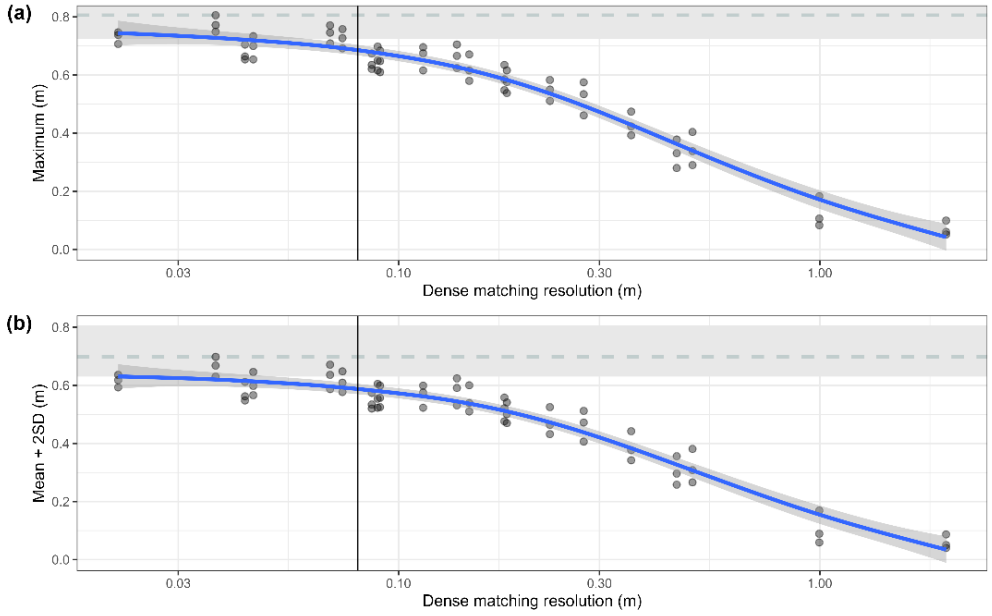

Figure 5. Relationship between dense matching resolution and height metrics for cases where the DTM was generated using the three best-performing ground filters (MTSO, LP1, LP2). (**a**) Median of maximum height observed for 299 shrubs. (**b**) Median of averaged height observed for 299 shrubs. In (**a**,**b**) the grey line and grey banner indicate the median and interquartile range of the maximum height (**a**) or the average canopy height (**b**) (mean + 2 standard deviations, conforming with upper

six branches) observed using the field-validated methods described in [35]. For both (**a**,**b**), metrics were calculated for unique subsets of ground filtering techniques and dense matching resolutions. Locally estimated scatterplot smoothing (LOESS) applied to visualize trends. Gray shading shows the 95% confidence interval of the standard error.

4. Discussion

The goal of this work was to test the replicability of DTMs and CHMs across different drone systems, sensors, dense matching resolutions, and bare ground classifiers to better understand the extent to which time-series analysis could be impacted by methodological effects instead of real environmental changes. Our results show that methodological effects introduced due to hardware and software factors have considerable potential to negatively affect the consistency and replicability of DTM and CHM models. Even though the highest Vegetated Vertical Accuracies achieved here (0.08 m RMSE) compare well with other works [4,20,25,26,47], we conclude that the expected best replicable performance under different conditions is closer to 0.1 m RMSE across a range of ground filtering approaches, and could, in fact, be much worse under certain conditions (e.g., 0.2 m RMSE in tall shrub patches). We further note that our highest reported DTM accuracies usually fall outside the interquartile range of observed RMSE distributions across a range of slightly differing scenarios due to differing resolutions of the source imagery, ground filtering approach, and/or dense matching settings (Figure 2e). As such, the highest reported VVA for specific workflows observed here (and likely elsewhere) should be seen as highly optimized anomalies that are not representative of future expected performance under differing conditions unless a great degree of experimentation and validation is undertaken. As DTMs are a prerequisite for CHMs, there is also considerable potential to introduce large systematic negative biases in site-level canopy height estimates and issues with temporal consistency of CHMs. Together, these results mean that methodological effects introduced due to hardware and software factors have considerable potential to negatively affect the consistency and replicability of DTM and CHM models, challenging the separability of real environmental change from time-series noise.

4.1. DTM Replicability

The results presented here highlight that consistent model performance across drone platforms and bare-earth classification approaches for Arctic shrublands is most likely if source imagery is collected with a spatial resolution of $\leq$1.5 cm and side-lap of >80%. The minimum resolution recommendation can be relaxed to $\leq$2.3 cm if the land-cover mainly constitutes shorter, less complex vegetation. During the data processing phase, a consistent performance improvement was observed (reductions up to 5 cm RMSE) when dense matching was performed at full image scales regardless of the point cloud classification approach following dense matching. Point cloud densification at full image scales computes additional 3D points compared to half image scales, requiring four times the amount of Random Access Memory (RAM) and substantially increased processing times. The observations in this study suggest DTM stability is nevertheless improved by these additional points, even though software manuals (e.g., Pix4D) indicate that these additional points are usually redundant. These findings apply to the consistency of VVA and the vegetative conditions found in the study area and may not apply in other vegetated terrain of substantially different vegetation compositions or in areas where bare ground exists (i.e., replicability of NVA). These observations expand upon earlier work by Refs. [35,48], which noted that only very-high-resolution imagery (0.5 cm) and high side-lap and point cloud densities enabled the creation of accurate DTMs ($\pm$0.08 m RMSE VVA) in areas with dense shrub cover and few ground gaps. We show that similar DTMs (median of $\pm$0.1 m RMSE) can be generated with imagery acquired at higher altitudes and slightly

coarser spatial resolutions (<2.3 cm) and processed at full image scales, thereby expanding the total coverage of data within the duration of a single drone flight. The better performance of TIN-based approaches observed in this study agrees with other studies in terrain with different vegetation types and geomorphic conditions [32]. In addition, we show that drone-based surveys can achieve VVAs (±0.1 m RMSE) comparable to low- or high-density Airborne Laser Scanning (Section 2.4), which further extends opportunities for stable elevation time-series.

An evaluation of a wide range of point cloud densities identified that 28 cm is an important dense matching resolution threshold beyond which DTM generation degrades considerably in this study area. This threshold relates to a minimum point density of 170 m^{-3}, following the observed negative power-law relationship between point cloud density and dense matching resolution (Equation (2)). This minimum point density can be achieved through a variety of survey setups and post-processing settings, for example, a 1.7 cm survey and a quarter dense matching scale or a 2.2 cm survey at half scale (Table 2). We therefore conclude that DTMs for stable elevation time-series are possible across different drone systems and sensors, after considering a minimum dense matching resolution of 28 cm and TIN-based lowest point filtering approaches. This important threshold may be different depending on the ecological setting and whether NVA or VVA is measured; therefore, threshold-based inquiries (Figures 3 and 5) based on the concept of the power-law relationship between point cloud density and dense matching resolution should be replicated in other shrub (and forested) domains. We conclude that knowledge of this threshold will help inform future site-specific monitoring requirements and gauges the likelihood of time-series susceptibility to methodological effects.

As reported elsewhere, vegetation cover was among the strongest explanatory variables of observed DTM RMSE, with higher RMSEs for dense dwarf birch and willow patches compared to other dwarf shrub and sedges across all source resolution classes. The vegetation cover in the study area is such that most areas between tall shrub canopies are covered by shorter dwarf shrubs (e.g., *Vaccinium uliginosum*, *V. vitis-idaea*, *Rhododendron subarcticum*) and moss, making true bare ground patches infrequent [35]. The absence of ground points explains the lower performance in these taller vegetation patches (often ≥0.2 m RMSE) compared to dwarf shrub patches (<0.2 m RMSE) no matter the source imagery resolution. These accuracies are similar to results achieved elsewhere in vegetated areas; for example, Refs. [30,49,50] observed increased elevation bias while ref. [51] noted an accuracy decrease of 0.1 m RMSE for every 20 cm increase in vegetation height. In the vegetation types in our study area, the ground filter approaches based on lowest point filtering outperformed other filtering techniques in terms of absolute accuracy (RMSE) and precision (IQR of RMSE). From an ecological perspective it also informs why the lowest point filtering (especially based on a 2 m window; LP2) outperformed other approaches in taller shrub environments as there is greater likelihood of finding neighboring points at similar elevations as below the shrub than when using other geometrical or morphological filtering techniques. The RMSE distributions observed in this study are likely worse than reported elsewhere because of the absence of "bare earth" conditions under the vegetative canopy. In permafrost regions there is often no solid ground to serve as basis for elevation measurements, which complicates validation activities and multi-temporal comparisons as the moss layer is partly penetrable by the GNSS rover rod if care is not taken [52]. Rod penetration of the moss surface is likely one of the reasons we observed positive biases in this study (Figure 2b), although positive biases are common to drone-derived DTMs in other vegetation settings as well [30,49,53]. Furthermore, sub-surface conditions in permafrost create highly variable micro-topography, such as mineral earth hummocks [54], challenging point-to-raster validation methods as the point-wise GNSS measurements

do not capture sub-grid topographic variability within the grid cell in question [55]. As point-to-grid validation techniques can yield RMSE values 20% higher than raster-to-raster validation of the same data [55], future work should include efforts to represent highly variable micro-topography more precisely in the validation process.

4.2. CHM Replicability

Drone surveys have been proposed as an ideal approach to scale between field data and satellite data to detect gradual changes in the composition, cover, and height of vegetation as it responds to climate or disturbance. The results of this study demonstrate that CHM metrics can be robustly derived (within ±5 cm of true site-level maximum heights) across source imagery resolutions < 1.5 cm if point clouds are produced at full-scale dense matching and robust ground filtering is used. If these conditions are met it is possible to derive median height estimates within 4–9% of the true (yet unknown) site-level median. Our analysis also shows that source imagery resolution plays a considerable role in reproducing site-level height estimates as the negative bias increases to 14% for 2–3 cm resolution imagery, and can be upwards of 50% for coarser resolution, even if robust ground filters are used. The use of coarse resolutions, half- or quarter-scale densification image scales, or sub-optimal ground filtering techniques will introduce even larger systematic biases in site-level shrub height estimates and issues with temporal consistency of CHM models. The experimental design of this study should be replicated across a range of vegetation compositions, as the results of this study are context dependent.

Average annual tundra shrub growth rates of 1–2 cm [38,39] and absolute uncertainties of ±5 cm in CHM metrics can be used to define signal-to-noise ratios (SNRs) and the minimum detectable change between surveys under ideal circumstances. At these growth rates, annual drone surveys of shrub heights have an SNR of 0.2 to 0.4, indicating no meaningful shrub growth information can be retrieved and that any observed signal is likely a fluctuation in noise rather than a real signal. A period of 2.5 to 5 years of average tundra shrub growth is therefore needed for the signal to equalize the measurement noise, and the period needs to be even longer for monitoring signals to be stronger than the background noise. On the other hand, useful monitoring periods shorten when annual vegetation growth rates exceed 1–2 cm (e.g., in wildfire scars, stable landslides, or drained lakes in the study area), or if disturbances cause large reductions in shrub height (e.g., 10–30 cm; [35]). Evidently, SNR worsens considerably where relative biases in CHM metrics increase from a best-case scenario of 4–9% to 14–50% of site-level medians. Ultimately, the acceptable SNR depends upon the user's error tolerance [56]. Knowledge of shrub height SNR is important as shrub height is one of the only physical traits of tundra vegetation that consistently changed in several decades of monitoring [21,22].

Decreasing point cloud densities because of coarsened source imagery resolution or larger densification scales have a reduced chance of accurately representing the base elevations of shrubs as well as shrub canopy geometries, as highlighted previously by [35] in the same study area or by [57] for small tree seedlings in boreal forests. Point clouds of vegetation features are known to "flatten" as source imagery coarsens or larger densification scales are used, thereby decreasing maximum and average heights. Drone photogrammetry is known to underestimate vegetation height in areas of dense vegetation, partially due to the flattening phenomena and because of ground occlusions [58,59]. In our study area, the main driver of smaller CHM estimates are ground surface errors (i.e., positive biases in DTM elevations at the base of shrubs) rather than canopy surface reconstructions (i.e., negative DSM biases; Figures S7 and S8). Recently, [14] observed similar explanatory power of regional shrub biomass models when using drone-derived photogrammetry with 1.7 cm imagery (5000–8000 points m^{-2}) or piloted airborne imagery of 3.1 cm spatial resolution

(500–2000 points m^{-2}). The latter densities are lower than the minimum point density advocated for in this work (±3219 m^{-3}; Equation (2); Figure 2a), but we note that the former imagery was collected by a consumer-grade camera while the latter imagery was collected by a medium-format metric camera. Metric cameras feature lower pixel densities and greater noise suppression that enable higher image quality and greater ability to resolve textures and contrasts [7], in turn increasing the availability of unique image features that increase point densities per unit of spatial resolution [60]. Therefore, as the coefficients for Equation (2) will be different for metric cameras compared to the 1″ and APC-size sensors used in this work there will also be different minimum dense matching scales and point density thresholds for metric cameras. This further underlines the context-dependency of this work, and this study encourages the replication of the presented experimental design in other environmental settings and with other hardware configurations.

4.3. Future Work

Several methodological solutions not investigated in this study may offer improved CHM accuracy and replicability and warrant further attention. One common approach is to apply a double grid survey approach (perpendicular flight lines) with slightly oblique imagery using convergent imaging geometry, as suggested by [61]. The addition of oblique imagery has been shown to improve DTM and CHM reconstructions elsewhere [20,62,63]. Others have achieved DTM improvements by means of spectral filtering [30,64] or by filtering point clouds by land-cover data [16]. These approaches will be sensitive to phenological conditions that challenge the identification of spectral cut-offs or land-cover classes when adopted for operational monitoring between sites. Less well known is the performance of multi-scale dimensionality filters [65] and point-cloud-optimized deep learning algorithms for DTM and CHM production, the replicability of which should be further tested in varying ecological conditions [66–68]. From a monitoring perspective, further quantitative analyses are needed that review environmental factors (e.g., illumination conditions, wind), as well as linking SNR variations to model performance and contextualizing these based on common vegetation growth rates. Finally, based on our results we call for more systematic analyses similar to the presented experimental design to explore methodological effects from a replicability standpoint rather than a single-instance accuracy standpoint, the former being more meaningful to long-term monitoring and time-series developments.

5. Conclusions

There is a pressing need to better understand the replicability of drone-based DTMs and CHMs in consideration of changing sensors and methods that have the potential to introduce systematic shifts in estimated properties. These shifts in turn could influence conclusions inferred from multi-temporal observations by either overestimating the true changes or making changes undetectable. The goal of this work was to test the replicability of DTMs and CHMs across different drone systems, sensors, dense matching resolutions, and bare ground classifiers to better understand the extent to which time-series trends could be impacted by methodological effects, obscuring real environmental changes. We present a power-law relationship between point cloud density and dense matching resolution and show that 28 cm is an important point cloud dense matching resolution threshold (or minimum point density of 170 m^{-3}) for vegetated environments similar to our study area, beyond which DTM replicability degrades considerably. Canopy height metrics decreased beyond a dense matching resolution of 8 cm (or minimum point density of 3219 m^{-3}), highlighting an important scale threshold affecting CHM replicability.

We conclude that methodological effects introduced due to hardware and software factors have considerable potential to negatively affect the consistency and replicability of

DTM and CHM models. However, maintaining consistency between models developed by differing approaches remains possible. Consistent DTM performance (as measured by Vegetated Vertical Accuracy) is most likely when source imagery is acquired with a spatial resolution of $\leq$1.5 cm and side-lap is greater than 80%. Our analysis also shows that CHM metrics can be robustly derived across source imagery resolutions <1.5 cm if point clouds are produced at full-scale dense matching and filtered to retrieve the lowest points using simple Triangular Irregular Networks. In these cases, maximum shrub height estimates will be within 4–9% of true site-level heights. For CHMs the spatial resolution of source imagery has a significant impact on bias, which was $-$14% and $-$50% for 2–3 cm resolution or coarser 12.5 cm imagery, respectively. Based on these findings, we advocate for increased attention to replicability of drone-based DTM and CHM survey methods across slightly differing scenarios to maintain the ability to separate real environmental changes from noise as time-series densify due to an ever-expanding drone user base and methodological options.

Supplementary Materials: The following supporting information can be downloaded at: https://www.mdpi.com/article/10.3390/rs18040627/s1. Figure S1: Visual overview of datasets and types; Figure S2: RMSE distributions for each ground filter approach and densification image scale, by vegetation cover; Figure S3: DTM elevation profiles using highest RGB source imagery resolution; Figure S4: DTM elevation profiles using lowest RGB source imagery resolution; Figure S5: CHM distributions for maximum height; Figure S6: CHM distributions for mean height + 2SD; Figure S7: DSM elevation profiles; Figure S8: Median DTM and DSM differences compared to the benchmark.

Author Contributions: J.V.d.S.: Conceptualization, Methodology, Software, Data Curation, Investigation, Formal Analysis, Writing—Original Draft, Writing—Review and Editing. R.H.F.: Conceptualization, Methodology, Data Curation, Funding Acquisition, Supervision, Writing—Review and Editing. T.C.L.: Funding Acquisition, Project Administration, Data Curation, Supervision, Writing—Review and Editing. All authors have read and agreed to the published version of the manuscript.

Funding: Funding for this project was provided by Polar Knowledge Canada (POLAR) under project 1516-121, the Canadian Space Agency Government Related Initiatives Program (GRIP), an NSERC Discovery Grant (RGPIN 06210-2018: Lantz), and logistical support from the Polar Continental Shelf Project. This research has also been supported by the Department of Environment and Natural Resources Climate Change and the Northwest Territories Cumulative Impact Monitoring Program of the GNWT (grant nos. 164 and 186, Steven V. Kokelj); the Natural Science and Engineering Research Council of Canada; and the Polar Continental Shelf Program, Natural Resources Canada (projects 313-18, 316-19, 318-20, and 320-20 to Steven V. Kokelj).

Data Availability Statement: Data sets generated during the current study are available from the corresponding author on reasonable request.

Acknowledgments: This work is part of a long-term permafrost monitoring and research program within the Government of Northwest Territories (GNWT) and NWT Geological Survey (NWT Research license #16805). We are grateful to the Indigenous peoples of the Inuvialuit Settlement Region of the Northwest Territories for the opportunity to work collaboratively and to learn and gather knowledge on their lands. Long-term support from the Inuvik and Tuktoyaktuk Hunters and Trappers Committees, the Inuvialuit Joint Secretariat, the Inuvialuit Land Administration, the Inuvialuit Regional Corporation (Charles Klengenberg), and the Aurora Research Institute (Joel McAlister) is gratefully acknowledged. Field support from Chanda Brietzke, Steve Kokelj, Paige Bennett, Robin Felix, Ian Olthof, Yu Zhang, William Woodley, Kiyo Campbell, Tracey Proverbs, and Maliya Cassels is also sincerely acknowledged. University of Lethbridge provided access to commercial point cloud software. The drone surveys were acquired as a contribution to the High Latitude Drone Ecology Network (HiLDEN; https://arcticdrones.org, accessed on 8 February 2026). This study was approved by the Scientific Services Office, Government of the Northwest Territories (formerly Aurora College) under NWT Research License #16805.

Conflicts of Interest: The authors declare no conflicts of interest.

References

1. Cunliffe, A.M.; Brazier, R.E.; Anderson, K. Ultra-Fine Grain Landscape-Scale Quantification of Dryland Vegetation Structure with Drone-Acquired Structure-from-Motion Photogrammetry. *Remote Sens. Environ.* **2016**, *183*, 129–143. [CrossRef]
2. Fraser, R.H.; Van der Sluijs, J.; Hall, R. Calibrating Satellite-Based Indices of Burn Severity from UAV-Derived Metrics of a Burned Boreal Forest in NWT, Canada. *Remote Sens.* **2017**, *9*, 279. [CrossRef]
3. Macander, M.J.; Palm, E.C.; Frost, G.V.; Herriges, J.D.; Nelson, P.R.; Roland, C.; Russell, K.L.M.; Suitor, M.J.; Bentzen, T.W.; Joly, K.; et al. Lichen Cover Mapping for Caribou Ranges in Interior Alaska and Yukon. *Environ. Res. Lett.* **2020**, *15*, 055001. [CrossRef]
4. Van der Sluijs, J.; Kokelj, S.V.; Fraser, R.H.; Tunnicliffe, J.; Lacelle, D. Permafrost Terrain Dynamics and Infrastructure Impacts Revealed by UAV Photogrammetry and Thermal Imaging. *Remote Sens.* **2018**, *10*, 1734. [CrossRef]
5. Hugenholtz, C.H.; Whitehead, K.; Brown, O.W.; Barchyn, T.E.; Moorman, B.J.; LeClair, A.; Riddell, K.; Hamilton, T. Geomorphological Mapping with a Small Unmanned Aircraft System (sUAS): Feature Detection and Accuracy Assessment of a Photogrammetrically-Derived Digital Terrain Model. *Geomorphology* **2013**, *194*, 16–24. [CrossRef]
6. Whitehead, K.; Hugenholtz, C.H. Remote Sensing of the Environment with Small Unmanned Aircraft Systems (UASs), Part 1: A Review of Progress and Challenges. *J. Unmanned Veh. Syst.* **2014**, *2*, 69–85. [CrossRef]
7. Nex, F.; Armenakis, C.; Cramer, M.; Cucci, D.A.; Gerke, M.; Honkavaara, E.; Kukko, A.; Persello, C.; Skaloud, J. UAV in the Advent of the Twenties: Where We Stand and What Is Next. *ISPRS J. Photogramm. Remote Sens.* **2022**, *184*, 215–242. [CrossRef]
8. Eltner, A.; Kaiser, A.; Castillo, C.; Rock, G.; Neugirg, F.; Abellán, A. Image-Based Surface Reconstruction in Geomorphometry—Merits, Limits and Developments. *Earth Surf. Dyn.* **2016**, *4*, 359–389. [CrossRef]
9. Van der Sluijs, J.; Saiet, E.; Bakelaar, C.N.; Wentworth, A.; Fraser, R.H.; Kokelj, S.V. Beyond Visual-Line-of-Sight (BVLOS) Drone Operations for Environmental and Infrastructure Monitoring: A Case Study in Northwestern Canada. *Drone Syst. Appl.* **2023**, *11*, 1–15. [CrossRef]
10. Zmarz, A.; Rodzewicz, M.; Dąbski, M.; Karsznia, I.; Korczak-Abshire, M.; Chwedorzewska, K.J. Application of UAV BVLOS Remote Sensing Data for Multi-Faceted Analysis of Antarctic Ecosystem. *Remote Sens. Environ.* **2018**, *217*, 375–388. [CrossRef]
11. Van der Sluijs, J.; Saiet, E.; Fraser, R.H.; Kokelj, S.V.; Bakelaar, C.N. Validation of beyond Visual-Line-of-Sight Drone Photogrammetry for Terrain and Canopy Height Applications. *Remote Sens. Appl. Soc. Environ.* **2024**, *35*, 101266. [CrossRef]
12. Frey, J.; Kovach, K.; Stemmler, S.; Koch, B. UAV Photogrammetry of Forests as a Vulnerable Process. A Sensitivity Analysis for a Structure from Motion RGB-Image Pipeline. *Remote Sens.* **2018**, *10*, 912. [CrossRef]
13. Howe, C.; Tullis, J.A. Context for Reproducibility and Replicability in Geospatial Unmanned Aircraft Systems. *Remote Sens.* **2022**, *14*, 4304. [CrossRef]
14. Alonzo, M.; Dial, R.J.; Schulz, B.K.; Andersen, H.-E.; Lewis-Clark, E.; Cook, B.D.; Morton, D.C. Mapping Tall Shrub Biomass in Alaska at Landscape Scale Using Structure-from-Motion Photogrammetry and Lidar. *Remote Sens. Environ.* **2020**, *245*, 111841. [CrossRef]
15. Cunliffe, A.M.; Assmann, J.J.; Daskalova, G.N.; Kerby, J.T.; Myers-Smith, I.H. Aboveground Biomass Corresponds Strongly with Drone-Derived Canopy Height but Weakly with Greenness (NDVI) in a Shrub Tundra Landscape. *Environ. Res. Lett.* **2020**, *15*, 125004. [CrossRef]
16. Orndahl, K.M.; Ehlers, L.P.W.; Herriges, J.D.; Pernick, R.E.; Hebblewhite, M.; Goetz, S.J. Mapping Tundra Ecosystem Plant Functional Type Cover, Height, and Aboveground Biomass in Alaska and Northwest Canada Using Unmanned Aerial Vehicles. *Arct. Sci.* **2022**, *8*, 1165–1180. [CrossRef]
17. Travers-Smith, H.; Coops, N.C.; Lantz, T.C.; Hamp, M.; Ignace, D.; Wulder, M.A.; Van der Sluijs, J. Vegetation Structure and Soil Organic Carbon Storage across Northern Forest-Tundra Ecotones in Continuous Permafrost. *Arct. Sci.* **2025**, *11*, 1–18. [CrossRef]
18. Humphries, J.K.; Van der Sluijs, J.; Morse, P.D.; Kokelj, S.V. Embankment Evolution of a Gravel Road on Permafrost Terrain Five Years after Construction: The Inuvik-Tuktoyaktuk Highway. In *Proceedings of the 12th International Conference on Permafrost (ICOP2024), Whitehorse, YT, Canada, 16–20 June 2024*; International Permafrost Association: Potsdam, Germany, 2024.
19. Dai, C.; Howat, I.M.; Van der Sluijs, J.; Liljedahl, A.K.; Higman, B.; Freymueller, J.T.; Ward Jones, M.K.; Kokelj, S.V.; Boike, J.; Walker, B.; et al. Applications of ArcticDEM for Measuring Volcanic Dynamics, Landslides, Retrogressive Thaw Slumps, Snowdrifts, and Vegetation Heights. *Sci. Remote Sens.* **2024**, *9*, 100130. [CrossRef]
20. Fraser, R.H.; Leblanc, S.; Prevost, C.; Van der Sluijs, J. Towards Precise Drone-Based Measurement of Elevation Change in Permafrost Terrain Experiencing Thaw and Thermokarst. *Drone Syst. Appl.* **2022**, *10*, 406–426. [CrossRef]
21. Bjorkman, A.D.; Myers-Smith, I.H.; Elmendorf, S.C.; Normand, S.; Rüger, N.; Beck, P.S.A.; Blach-Overgaard, A.; Blok, D.; Cornelissen, J.H.C.; Forbes, B.C.; et al. Plant Functional Trait Change across a Warming Tundra Biome. *Nature* **2018**, *562*, 57–62. [CrossRef]

22. Myers-Smith, I.H.; Grabowski, M.M.; Thomas, H.J.D.; Angers-Blondin, S.; Daskalova, G.N.; Bjorkman, A.D.; Cunliffe, A.M.; Assmann, J.J.; Boyle, J.S.; McLeod, E.; et al. Eighteen Years of Ecological Monitoring Reveals Multiple Lines of Evidence for Tundra Vegetation Change. *Ecol. Monogr.* **2019**, *89*, e01351. [CrossRef]
23. IPCC. Summary for Policymakers. In *Climate Change 2022: Impacts, Adaptation and Vulnerability*; Contribution of Working Group II to the Sixth Assessment Report of the Intergovernmental Panel on Climate Change; Cambridge University Press: Cambridge, UK; New York, NY, USA, 2022.
24. Burn, C.R.; Bartsch, A.; Chakraborty, E.; Das, S.; Frauenfelder, R.; Gärtner-Roer, I.; Gisnås, K.G.; Herring, T.; Jones, B.M.; Kokelj, S.V.; et al. Developments in Permafrost Science and Engineering in Response to Climate Warming in Circumpolar and High Mountain Regions, 2019–2024. *Permafr. Periglac. Process.* **2025**, *36*, 167–188. [CrossRef]
25. James, M.R.; Robson, S.; d'Oleire-Oltmanns, S.; Niethammer, U. Optimising UAV Topographic Surveys Processed with Structure-from-Motion: Ground Control Quality, Quantity and Bundle Adjustment. *Geomorphology* **2017**, *280*, 51–66. [CrossRef]
26. Tonkin, T.; Midgley, N. Ground-Control Networks for Image Based Surface Reconstruction: An Investigation of Optimum Survey Designs Using UAV Derived Imagery and Structure-from-Motion Photogrammetry. *Remote Sens.* **2016**, *8*, 786. [CrossRef]
27. Wiseman, D.; Van der Sluijs, J. Alternative Methods for Developing and Assessing the Accuracy of UAV-Derived DEMs. *Int. J. Appl. Geospat. Res.* **2015**, *6*, 58–77. [CrossRef]
28. Martínez-Carricondo, P.; Agüera-Vega, F.; Carvajal-Ramírez, F.; Mesas-Carrascosa, F.-J.; García-Ferrer, A.; Pérez-Porras, F.-J. Assessment of UAV-Photogrammetric Mapping Accuracy Based on Variation of Ground Control Points. *Int. J. Appl. Earth Obs. Geoinf.* **2018**, *72*, 1–10. [CrossRef]
29. Sanz-Ablanedo, E.; Chandler, J.H.; Rodríguez-Pérez, J.R.; Ordóñez, C. Accuracy of Unmanned Aerial Vehicle (UAV) and SfM Photogrammetry Survey as a Function of the Number and Location of Ground Control Points Used. *Remote Sens.* **2018**, *10*, 1606. [CrossRef]
30. Anders, N.; Valente, J.; Masselink, R.; Keesstra, S. Comparing Filtering Techniques for Removing Vegetation from UAV-Based Photogrammetric Point Clouds. *Drones* **2019**, *3*, 61. [CrossRef]
31. Şerifoğlu Yilmaz, C.; Yilmaz, V.; Güngör, O. Investigating the Performances of Commercial and Non-Commercial Software for Ground Filtering of UAV-Based Point Clouds. *Int. J. Remote Sens.* **2018**, *39*, 5016–5042. [CrossRef]
32. Štroner, M.; Urban, R.; Línková, L. Multidirectional Shift Rasterization (MDSR) Algorithm for Effective Identification of Ground in Dense Point Clouds. *Remote Sens.* **2022**, *14*, 4916. [CrossRef]
33. Cunliffe, A.M.; Anderson, K.; Boschetti, F.; Brazier, R.E.; Graham, H.A.; Myers-Smith, I.H.; Astor, T.; Boer, M.M.; Calvo, L.G.; Clark, P.E.; et al. Global Application of an Unoccupied Aerial Vehicle Photogrammetry Protocol for Predicting Aboveground Biomass in Non-Forest Ecosystems. *Remote Sens. Ecol. Conserv.* **2022**, *8*, 57–71. [CrossRef] [PubMed]
34. Graham, A.N.V.; Coops, N.C.; Tompalski, P.; Plowright, A.; Wilcox, M. Effect of Ground Surface Interpolation Methods on the Accuracy of Forest Attribute Modelling Using Unmanned Aerial Systems-Based Digital Aerial Photogrammetry. *Int. J. Remote Sens.* **2020**, *41*, 3287–3306. [CrossRef]
35. Fraser, R.H.; Olthof, I.; Lantz, T.C.; Schmitt, C. UAV Photogrammetry for Mapping Vegetation in the Low-Arctic. *Arct. Sci.* **2016**, *2*, 79–102. [CrossRef]
36. Ecosystem Classification Group. *Ecological Regions of the Northwest Territories—Southern Arctic*; Government of the Northwest Territories: Yellowknife, NT, Canada, 2012; pp. 1–170.
37. Burn, C.R.; Kokelj, S.V. The Environment and Permafrost of the Mackenzie Delta Area. *Permafr. Periglac. Process.* **2009**, *20*, 83–105. [CrossRef]
38. Lantz, T.C.; Gergel, S.E.; Kokelj, S.V. Spatial Heterogeneity in the Shrub Tundra Ecotone in the Mackenzie Delta Region, Northwest Territories: Implications for Arctic Environmental Change. *Ecosystems* **2010**, *13*, 194–204. [CrossRef]
39. Myers-Smith, I.H.; Hik, D.S.; Kennedy, C.; Cooley, D.; Johnstone, J.F.; Kenney, A.J.; Krebs, C.J. Expansion of Canopy-Forming Willows Over the Twentieth Century on Herschel Island, Yukon Territory, Canada. *Ambio* **2011**, *40*, 610–623. [CrossRef]
40. Axelsson, P.; Fritsch, D.; Molenaar, M. DEM Generation from Laser Scanner Data Using Adaptive TIN Models. *Int. Arch. Photogramm. Remote Sens.* **2000**, *33*, 110–117.
41. Zhang, K.; Chen, S.-C.; Whitman, D.; Shyu, M.-L.; Yan, J.; Zhang, C. A Progressive Morphological Filter for Removing Nonground Measurements from Airborne LIDAR Data. *IEEE Trans. Geosci. Remote Sens.* **2003**, *41*, 872–882. [CrossRef]
42. Pingel, T.J.; Clarke, K.C.; McBride, W.A. An Improved Simple Morphological Filter for the Terrain Classification of Airborne LIDAR Data. *ISPRS J. Photogramm. Remote Sens.* **2013**, *77*, 21–30. [CrossRef]
43. Zhang, W.; Qi, J.; Wan, P.; Wang, H.; Xie, D.; Wang, X.; Yan, G. An Easy-to-Use Airborne LiDAR Data Filtering Method Based on Cloth Simulation. *Remote Sens.* **2016**, *8*, 501. [CrossRef]
44. St-Onge, B.; Vega, C.; Fournier, R.A.; Hu, Y. Mapping Canopy Height Using a Combination of Digital Stereo-photogrammetry and Lidar. *Int. J. Remote Sens.* **2008**, *29*, 3343–3364. [CrossRef]
45. Popescu, S.C.; Wynne, R.H. Seeing the Trees in the Forest. *Photogramm. Eng. Remote Sens.* **2004**, *70*, 589–604. [CrossRef]

46. American Society for Photogrammetry and Remote Sensing. ASPRS Positional Accuracy Standards for Geospatial Data, Edition 2, Version 1.0. *Photogramm. Eng. Remote Sens.* **2023**, *89*, 589–592. [CrossRef]
47. Hugenholtz, C.; Brown, O.; Walker, J.; Barchyn, T.; Nesbit, P.; Kucharczyk, M.; Myshak, S. Spatial Accuracy of UAV-Derived Orthoimagery and Topography: Comparing Photogrammetric Models Processed with Direct Geo-Referencing and Ground Control Points. *Geomatica* **2016**, *70*, 21–30. [CrossRef]
48. Fraser, R.H.; Lantz, T.C.; McFarlane-Winchester, M.; Van der Sluijs, J.; Prévost, C.L. *Testing the Potential of UAV Photogrammetry for Deriving Bare Earth Models in Arctic Shrublands*; Geomatics Canada Open File 54; Natural Resources Canada: Ottawa, ON, Canada, 2020; p. 20.
49. Wallace, L.; Lucieer, A.; Malenovský, Z.; Turner, D.; Vopěnka, P. Assessment of Forest Structure Using Two UAV Techniques: A Comparison of Airborne Laser Scanning and Structure from Motion (SfM) Point Clouds. *Forests* **2016**, *7*, 62. [CrossRef]
50. Lovitt, J.; Rahman, M.M.; McDermid, G.J. Assessing the Value of UAV Photogrammetry for Characterizing Terrain in Complex Peatlands. *Remote Sens.* **2017**, *9*, 715. [CrossRef]
51. Salach, A.; Bakuła, K.; Pilarska, M.; Ostrowski, W.; Górski, K.; Kurczyński, Z. Accuracy Assessment of Point Clouds from LiDAR and Dense Image Matching Acquired Using the UAV Platform for DTM Creation. *ISPRS Int. J. Geo-Inf.* **2018**, *7*, 342. [CrossRef]
52. Anders, K.; Marx, S.; Boike, J.; Herfort, B.; Wilcox, E.J.; Langer, M.; Marsh, P.; Höfle, B. Multitemporal Terrestrial Laser Scanning Point Clouds for Thaw Subsidence Observation at Arctic Permafrost Monitoring Sites. *Earth Surf. Process. Landf.* **2020**, *45*, 1589–1600. [CrossRef]
53. Jensen, J.L.R.; Mathews, A.J. Assessment of Image-Based Point Cloud Products to Generate a Bare Earth Surface and Estimate Canopy Heights in a Woodland Ecosystem. *Remote Sens.* **2016**, *8*, 50. [CrossRef]
54. Kokelj, S.V.; Burn, C.R.; Tarnocai, C. The Structure and Dynamics of Earth Hummocks in the Subarctic Forest near Inuvik, Northwest Territories, Canada. *Arct. Antarct. Alp. Res.* **2007**, *39*, 99–109. [CrossRef]
55. Smith, M.W.; Carrivick, J.L.; Quincey, D.J. Structure from Motion Photogrammetry in Physical Geography. *Prog. Phys. Geogr. Earth Environ.* **2016**, *40*, 247–275. [CrossRef]
56. Rose, A. (Ed.) Human Vision. In *Vision: Human and Electronic*; Springer: Boston, MA, USA, 1973; pp. 29–53.
57. Castilla, G.; Filiatrault, M.; McDermid, G.J.; Gartrell, M. Estimating Individual Conifer Seedling Height Using Drone-Based Image Point Clouds. *Forests* **2020**, *11*, 924. [CrossRef]
58. Chen, S.; McDermid, G.J.; Castilla, G.; Linke, J. Measuring Vegetation Height in Linear Disturbances in the Boreal Forest with UAV Photogrammetry. *Remote Sens.* **2017**, *9*, 1257. [CrossRef]
59. Mestre-Runge, C.; Ludwig, M.; Sebastià, M.T.; Plaixats, J.; Lobo, A. Optimizing Drone-Based Surface Models for Prescribed Fire Monitoring. *Fire* **2023**, *6*, 419. [CrossRef]
60. Dandois, J.P.; Baker, M.; Olano, M.; Parker, G.G.; Ellis, E.C. What Is the Point? Evaluating the Structure, Color, and Semantic Traits of Computer Vision Point Clouds of Vegetation. *Remote Sens.* **2017**, *9*, 355. [CrossRef]
61. James, M.R.; Robson, S. Mitigating Systematic Error in Topographic Models Derived from UAV and Ground-Based Image Networks. *Earth Surf. Process. Landf.* **2014**, *39*, 1413–1420. [CrossRef]
62. Díaz, G.M.; Mohr-Bell, D.; Garrett, M.; Muñoz, L.; Lencinas, J.D. Customizing Unmanned Aircraft Systems to Reduce Forest Inventory Costs: Can Oblique Images Substantially Improve the 3D Reconstruction of the Canopy? *Int. J. Remote Sens.* **2020**, *41*, 3480–3510. [CrossRef]
63. Wallace, L.; Bellman, C.; Hally, B.; Hernandez, J.; Jones, S.; Hillman, S. Assessing the Ability of Image Based Point Clouds Captured from a UAV to Measure the Terrain in the Presence of Canopy Cover. *Forests* **2019**, *10*, 284. [CrossRef]
64. Tan, Y.; Wang, S.; Xu, B.; Zhang, J. An Improved Progressive Morphological Filter for UAV-Based Photogrammetric Point Clouds in River Bank Monitoring. *ISPRS J. Photogramm. Remote Sens.* **2018**, *146*, 421–429. [CrossRef]
65. Brodu, N.; Lague, D. 3D Terrestrial Lidar Data Classification of Complex Natural Scenes Using a Multi-Scale Dimensionality Criterion: Applications in Geomorphology. *ISPRS J. Photogramm. Remote Sens.* **2012**, *68*, 121–134. [CrossRef]
66. Diab, A.; Kashef, R.; Shaker, A. Deep Learning for LiDAR Point Cloud Classification in Remote Sensing. *Sensors* **2022**, *22*, 7868. [CrossRef]
67. Fareed, N.; Flores, J.P.; Das, A.K. Analysis of UAS-LiDAR Ground Points Classification in Agricultural Fields Using Traditional Algorithms and PointCNN. *Remote Sens.* **2023**, *15*, 483. [CrossRef]
68. Gevaert, C.M.; Persello, C.; Nex, F.; Vosselman, G. A Deep Learning Approach to DTM Extraction from Imagery Using Rule-Based Training Labels. *ISPRS J. Photogramm. Remote Sens.* **2018**, *142*, 106–123. [CrossRef]

Disclaimer/Publisher's Note: The statements, opinions and data contained in all publications are solely those of the individual author(s) and contributor(s) and not of MDPI and/or the editor(s). MDPI and/or the editor(s) disclaim responsibility for any injury to people or property resulting from any ideas, methods, instructions or products referred to in the content.